scientific **data**

OPEN

DATA DESCRIPTOR

High-resolution ocean color imagery from the SeaHawk-HawkEye CubeSat mission

Philip J. Bresnahan [1,2 ✉], Sara Rivero-Calle [3], John Morrison[2], Gene Feldman[4], Alan Holmes[5], Sean Bailey [4], Alicia Scott[4,6], Liang Hong[4], Frederick Patt[4,6], Norman Kuring[4], Corrine Rojas[4,6], Craig Clark[7,8], John Charlick [7], Baptiste Lombard[7], Hessel Gorter [7], Roberto Travaglini[7] & Hazel Jeffrey[7]

Here we describe the data obtained by a successful proof-of-concept initiative to launch the first ocean color imager on board a CubeSat satellite and collect research-grade imagery at severalfold higher spatial resolution than any other ocean color satellite mission. The 3U CubeSat, named SeaHawk, flew at a nominal altitude of 585 km. Its ocean color sensor, HawkEye, collected 7,471 research-grade push-broom images of $230 \times 780\,km^2$ at best-in-class $130 \times 130\,m^2$ per pixel. The sensor is built with comparatively low-cost commercial off-the-shelf optoelectronics and was designed to match NASA SeaWiFS ocean color specifications, including wavelengths, bandwidths, and signal-to-noise ratios. HawkEye's design for ocean color remote sensing combined with its high spatial resolution make the imagery especially well-suited for coastal, estuarine, and limnological applications. Ultimately, the successful mission provided open access to a rich global dataset of calibrated and quality-controlled imagery for use in aquatic ecology and environmental change studies.

Background & Summary

Satellite remote sensing has been shown to be highly effective at mapping environmental change over large spatial extents and for extended durations[1]. Ocean color remote sensing is the subdomain of remote sensing wherein specific wavelengths of light in the visible to near-infrared spectrum are collected with the goal of determining the abundance of optically active constituents—including chlorophyll-a, suspended sediments, and colored dissolved organic matter—in surface waters of aquatic ecosystems[2]. Monitoring these parameters provides critical insights into, for example, algae growth, eutrophication, harmful algal blooms, sediment transport, light availability, and terrestrial runoff, especially near highly developed urban and agricultural lands[3]. Water quality monitoring is also tied to mandates for multiple Sustainable Development Goals (SDGs): especially Goal 6's ("water and sanitation") Indicator 6.3.2 ("proportion of bodies of water with good ambient water quality"), and Goal 14's ("life below water") Indicator 14.1.1 ("(a) index of coastal eutrophication")[4]. Given the various needs for monitoring water quality and satellite remote sensing's unique capacity to meet the demand of global, high spatial resolution coverage, the US National Academy of Sciences has highlighted the need for sustained ocean color observations[2].

Ocean color remote sensing includes drone-based measurements[5–7], but we focus on satellite-borne sensors here. We also note that these aquatic ecosystems need not be oceanic as the techniques also apply to brackish and freshwater systems where the water depth is greater than the optical depth, yet "ocean color" remains the most common name. NASA's first satellite ocean color mission, the Coastal Zone Color Scanner, proved the concept in the 1980s[8] and, in recent decades, there have been numerous successful government-funded ocean color missions, such as NASA's SeaWiFS, MODIS-Aqua and Terra, and PACE, NOAA's VIIRS, the European Space Agency's MERIS and Sentinel-3 OLCI. These sensors range in spatial resolution (from 300 m to 1,100 m

[1]Department of Earth and Ocean Sciences, University of North Carolina Wilmington, Wilmington, NC, USA. [2]Center for Marine Science, University of North Carolina Wilmington, Wilmington, NC, USA. [3]Skidaway Institute of Oceanography, University of Georgia, Savannah, GA, USA. [4]NASA Goddard Space Flight Center, Greenbelt, MD, USA. [5]Cloudland Instruments, Inc, Santa Barbara, CA, USA. [6]Science Application International Corp., Greenbelt, MD, USA. [7]Formerly at AAC Clyde Space, Glasgow, Scotland, UK. [8]University of Strathclyde, Glasgow, Scotland, UK. ✉e-mail: bresnahanp@uncw.edu

per pixel) and revisit time (daily to several weeks), and all have contributed to massive gains in understanding of sea surface variability, especially in the domains of biological productivity[9–11], carbon cycling[12,13], and turbidity/sediment transport[14–16].

Other missions with higher spatial resolution but not specified for ocean color, such as Landsat 8 and 9's Operational Land Imager (OLI) and Sentinel-2 A and B's MultiSpectral Instrument (MSI) have demonstrated the ability to conduct similar research in aquatic settings using higher spatial resolution sensors designed primarily for terrestrial applications (e.g., 10–60 m per pixel)[17–21]. Even higher spatial resolution imagery (e.g., 1–5 m) from commercial CubeSats such as Planet has been used to estimate aquatic chlorophyll and turbidity patterns[22] and demonstrate the potential for conducting highly spatially and temporally resolved analyses from a constellation of satellite imagers[23]. However, these sensors with resolution of order one meter to tens of meters were not optimized for ocean color sensing and, in optically complex waters where absorption and scattering may be highly variable due to a wide range of suspended and dissolved constituents and land adjacency/bottom reflectance effects, they are less capable of distinguishing and quantifying those constituents. For instance, Manzo *et al.*[24] describe challenges with estimating colored dissolved organic matter and Pahlevan *et al.*[19] report occasional negative retrievals of remote sensing reflectance (rendering aquatic constituent calculations challenging or impossible), both with Landsat and Sentinel products.

These missions leave a gap in coastal and estuarine satellite ocean color analysis where an optimal pairing of spatial resolution and spectral quality are required to resolve finer spatial variability in optically complex waters and to get closer to coastlines without mixed water/land or benthos pixels. Moreover, the Planet constellations—comprising dozens of satellites—and the Landsat-Sentinel-2 "virtual constellation"—with four—demonstrate the utility of launching a multitude of satellites and imagers. Planet in particular has seen notable success through the use of cost-efficient CubeSats which are markedly less expensive to design, fabricate, and launch[25].

Due to the challenges with the coastal ocean's optical complexity and the relatively low signal returned from the ocean's surface to a satellite sensor (roughly 90% of photons are absorbed by the ocean or scattered by the atmosphere), ocean color remote sensing has especially stringent optical quality demands. Consequently, operational ocean color satellite remote sensing has to date been the domain of large, federally funded initiatives. Yet, given the increase in abundance and application of CubeSats, we sought to prove the concept that an ocean color quality imager could be constructed with commercial off-the-shelf parts, integrated into a CubeSat bus, and operationalized to meet the needs of the ocean color research community. Here we describe the SeaHawk-HawkEye mission's two years of operational ocean color data, and provide an example of HawkEye's unique ability to resolve finer spatial scale variability in optically complex coastal waters following Hurricane Ian (September 2022).

Methods

System design. The SeaHawk-HawkEye mission is a government-industry-academia collaboration with partners including the University of North Carolina Wilmington, University of Georgia, NASA Goddard Spaceflight Center, Cloudland Instruments, and Clyde Space. The satellite bus, named SeaHawk, is a 3U CubeSat, or a $30 \times 10 \times 10 \, cm^3$ platform built by Clyde Space and was responsible for attitude monitoring and control, momentum management and fine-pointing for stable imaging, power management, image scheduling, and science data collection/downlink. Flight altitude and revisit period were 594 km and 18 days at launch, decaying to 574 km and 90 days by end of mission due to orbital drag. SeaHawk contains a 40 W-hr battery and four solar panels (only two of four deployed after launch, rendering the other two unusable). Engineering system data were uplinked from the ground to the satellite over Very High Frequency (VHF) radio at 1200 bps and downlinked over Ultra High Frequency (UHF) at 9600 bps. A Syrlinks X-band transmitter sent scientific data to two ground stations: one at Wallops Data Acquisition Station in Virginia, USA, and one at the Alaska Satellite Facility, Alaska, USA, both part of NASA's Near Earth Network. The Clyde Space motherboard also provided access to guidance and control sensors (3-axis magnetometers and gyroscopes, coarse and fine sun sensors, and GPS) and actuators (3-axis reaction wheels and magnetorquers for attitude control). The motherboard contained 1.8 GB data storage (sufficient for 18 100 MB images) and access to the HawkEye sensor package.

SeaHawk (Fig. 1) was launched 3-Dec-2018 aboard the SpaceX Spaceflight SSA-O SmallSat Express using a Falcon IX booster from Vandenberg Air Force Base, CA, USA. The first test image was collected on 21-Mar-2019, following repeated attempts to deploy the remaining two solar panels and operate the GPS receiver (both were unsuccessful). The commencement of routine science operations required that a number of additional technical issues be addressed, including: correcting the use of the fine Sun sensors by the attitude determination and control system (ADCS) software; calibrating the magnetometers; tuning the parameters for both the attitude determination Kalman filter and the control law to stabilize the pointing control; enabling momentum management to allow continued nadir pointing for image data collection without saturating the reaction wheels; and enabling station pointing during X-band downlinks to achieve reliable signal acquisition. Further capabilities were tested and verified for pitching the spacecraft during image acquisition to avoid Sun glint and rolling to allow imaging of the same location on multiple days as the orbit precessed. While its nominal return period was 18 days at launch, the mission also collected several sets of consecutive daily images of up to one week of the same location using this pointing control. This feature was predominantly used in a "proof of concept" capacity; however daily repeat images were occasionally requested when fieldwork was planned in order to improve temporal coverage and reduce the risk of missing an area due to cloud cover.

SeaHawk officially transitioned into its operational phase (after fine-pointing, geolocation, image downlinking, and calibration procedures were made robust) on 21-Jun-2021. Geolocation and data processing routines are described in greater detail below. Operations ended 27-Oct-2023 after the reaction wheels—responsible for 3-axis attitude control (i.e., one set of reaction wheels for each of the x, y, and z axes of the spacecraft)—began
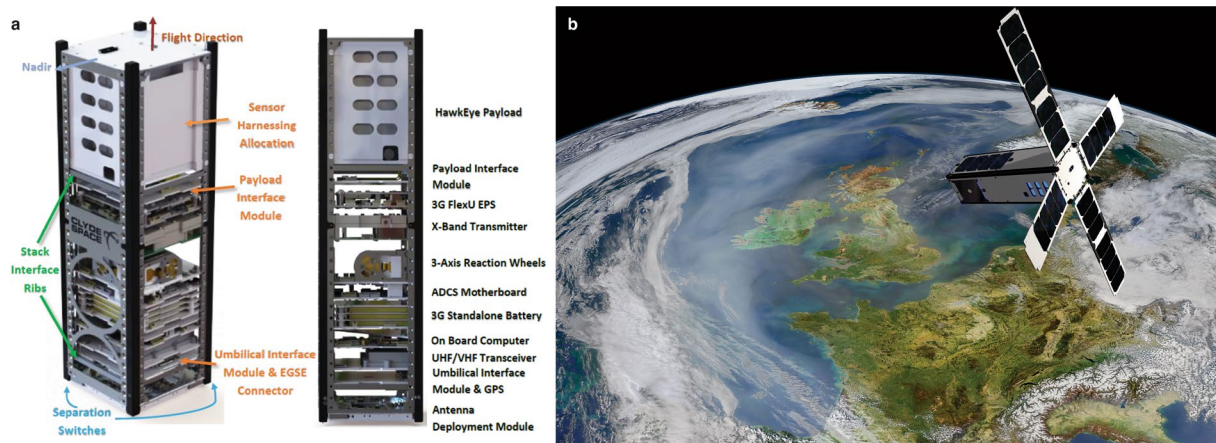
Fig. 1 (**a**) SeaHawk's major system components and depiction of flight direction and orientation during Earth imaging. Solar panels not shown. (**b**) Rendering of SeaHawk with four solar panels deployed.

to seize frequently, resulting in the loss of fine-pointing and, consequently, twisted or stretched images, images pointing in the wrong direction, lost images, and issues with data downlinking.

The sensor, HawkEye, is a multispectral imager designed and built by Cloudland Instruments to match the specifications (wavelengths and wavelength-dependent sensitivities) of the NASA SeaWiFS mission. Specifically, bands of 412, 443, 490, 510, 555, 670, 750.9, and 865 nm were selected. Notably, HawkEye implements commercial off-the-shelf charge-coupled device (CCD) arrays (Onsemi KLI-4104), which meaningfully decreased the cost and timeline of development. The HawkEye instrument consists of four CCD arrays with two bandpass filters per array to provide the 8 spectral bands for the sensor. Each band consists of 1,800 illuminated elements which collected push-broom images, resulting in scenes 1,800 pixels wide × 6,000 pixels long ($230 \times 780\,km^2$ at average mission altitude). Each pixel comprises four samples at each wavelength; that is, every final recorded value is the sum of four readings as the instrument rapidly samples the same location before moving to the next scan. The instrument was designed with the ability to record each pixel in three separate channels of its CCD array, thus effectively oversampling by a factor of 12 (4 readings × 3 channels per pixel) to improve the signal to noise ratio (SNR) by a factor of $\sqrt{12} \approx 3.5$. The sensor also contained a shutter which can be closed to allow HawkEye to collect dark data which is used to remove thermal noise from the data. Finally, HawkEye's exposure settings (optics transmission and electronics gain settings) were tuned such that bright clouds and coastal features would not oversaturate the detector and cause "blooming," wherein light from adjacent pixels can cause nearby darker pixels to falsely record brighter signals. In combination with HawkEye's high spatial resolution, this feature allows analysis of water very close to clouds and coastlines with less concern for these adjacency effects. Further details on HawkEye instrument development and on-ground characterization are available in Holmes, *et al.*[26].

Data transmission and processing. Data storage and transmission limitations allowed the collection of nominally 18 images per day. The University of Georgia, NASA Goddard, and Clyde Space coordinated image scheduling (Fig. 2) to meet scientific objectives (including allowing the international scientific community to request images from regions of interest via a UNC Wilmington web portal). HawkEye data were downlinked to NASA and processed by the Ocean Biology Processing Group at NASA Goddard following published routines (see detail below). HawkEye data processing is also built into NASA's freely available and widely used SeaDAS software[27] and ocean color science software (ocssw).

Atmospheric correction (i.e., the estimation and removal of the portion of the signal due to atmospheric scattering from the satellite's received signal) typically relies on signal in the near infrared (NIR) bands (following, e.g., Gordon and Wang[28] and Gordon[29]). However, HawkEye experienced apparent erosion of anti-reflection coatings on the exterior surface of the polarization scrambler due to unstable attitude control early in the SeaHawk mission. Poor attitude control resulted in the sensor pointing directly at the Sun and in the flight direction, thus subjecting it temporarily to hazardous conditions. Consequently, the NIR signals experienced a so-called "ghosting" issue wherein a "ghost" of the actual image was reflected/transposed at a lower but non-negligible intensity into a different section of the "true" image, thus skewing results. The ghost was not visible in the initial images from orbit, increased to 1.5% of the true image's intensity on 15-June-2020, and to 2.9% on 24-May-2021.

To circumvent the issues with its NIR bands, HawkEye atmospheric correction borrows from the technique used for NASA's first ocean color mission (the Coastal Zone Color Scanner or CZCS) which employs the 670 nm band and a simpler, single aerosol model, described as yielding remarkable correspondence between that mission and modern sensors[30]. Following atmospheric correction, which allows calculation of remote sensing reflectances at each measured wavelength ($R_{rs}(\lambda)$), standard bio-optical algorithms are used to calculate geophysical parameters, such as chlorophyll-a concentration, diffuse attenuation, inherent optical properties (absorption and backscattering), and others following IOCCG[31], Werdell, *et al.*[32], O'Reilly and Werdell[33], and references therein.
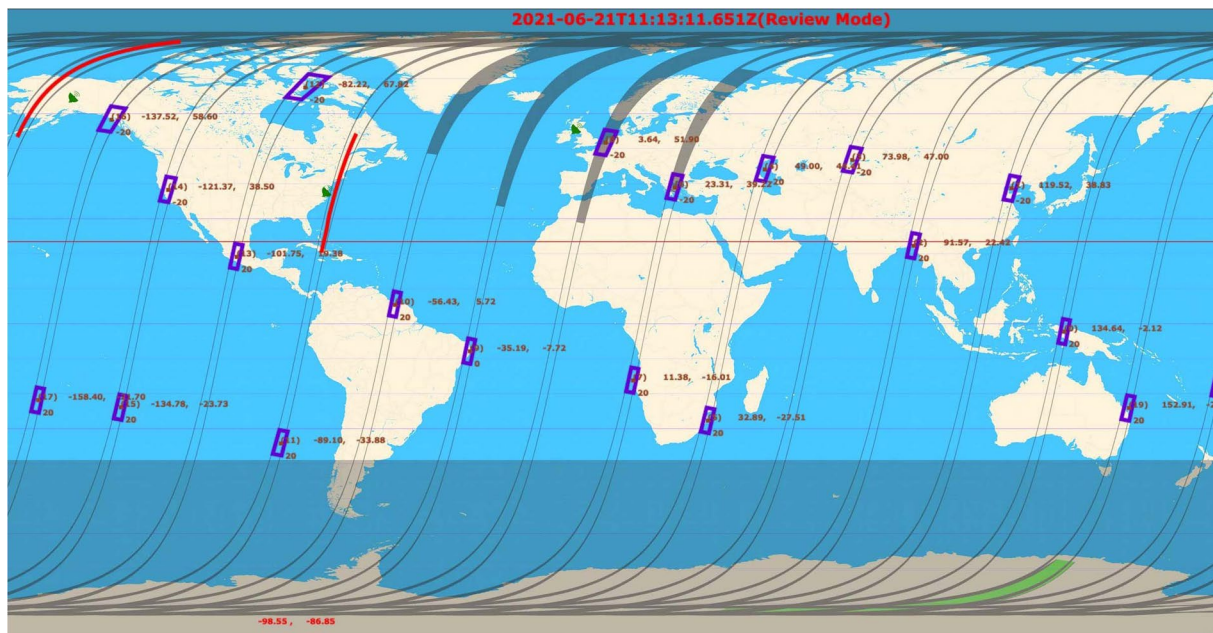
Fig. 2 Representative HawkEye imaging schedule, 21-Jun-2021. Blue rectangles represent locations where images were scheduled to be captured on that day. Satellite receiver icons in VA and AK, USA, depict data downlink stations and red lines illustrate satellite's position relative to the Earth's surface during downlink.

Since there are four separate CCDs, each supporting two spectral bands, the data from each band are slightly offset in both the along-track and cross-track directions, and are therefore registered to a common reference band. Additionally, the focal length varies slightly from band to band. Corrections for the physical offsets and the focal length differences are necessary to ensure that the data from each pixel for each band match the same geolocated area in the scene. A manual tuning of the imagery's geolocation was also required. The HawkEye sensor's ground resolution was superior to the SeaHawk spacecraft's ability to quantify its own pointing (130 m corresponds to 0.0125° angular resolution, smaller than the satellite's knowledge of its orientation). Furthermore, the spacecraft's GPS antenna never properly functioned for unknown reasons and SeaHawk's magnetometer was only accurate to 1–2°. Spacecraft attitude sensors were sampled at 1 Hz and post-processed to model SeaHawk's motion during pointing, but absolute accuracy was insufficient for scientific image analysis. As a result, image geolocation could not be automated, resulting in the need for a manual geolocation correction. The NASA Goddard team employed a web-based tool initially developed for the same purpose for the Hyperspectral Imager for the Coastal Ocean (HICO) mission which allowed an analyst to manually align the collected image's coastline with a high-resolution coastline map to retrieve a more accurate geolocation.

Data Records

The full dataset is available at NASA Goddard's Ocean Biology Distributed Active Archive Center (OB.DAAC) and NASA's Earthdata browser (https://search.earthdata.nasa.gov/search?fi=HawkEye, with access to L1 data/metadata[34] at https://doi.org/10.5067/SEAHAWK-1/HawkEye/L1A/DATA/1, and L2 data/metadata[35] at https://doi.org/10.5067/SEAHAWK-1/HawkEye/L2/OC/2022.0, accessed 18-Oct-2024). Data are packaged in Network Common Data Form 4 (NetCDF4) by the NASA Goddard Space Flight Center's Ocean Data Processing System. L1 data include geolocation data ("navigation_data": e.g., latitude, longitude, time, spacecraft roll), sensor metadata ("parameters_telemetry_data": e.g., software version, circuitry temperatures and voltages, exposure and binning settings), and sensor data ("earth_view_data": e.g., engineering counts at each pixel for each wavelength as well as dark counts when the shutter is closed). L2 data similarly include geolocation data as well as atmospheric correction and calibration data ("sensor_band_parameters"), processing software metadata ("processing_control": e.g., SeaDAS software version, input data such as HawkEye L1 data, meteorology and climatology data, and look-up tables), and geophysical data ("geophysical_data": e.g., aerosol properties, remote sensing reflectances at each wavelength, chlorophyll-a concentration, diffuse attenuation coefficient for downwelling irradiance at 490 nm, particulate inorganic carbon concentration, particulate organic carbon concentration, and any flags that were raised in L1-to-L2 processing). The file naming convention is MMMM_IIII. YYYYMMDDTHHMMSS.LLLL.SSSS.VVVVVV.nc where MMMM represents mission (SeaHawk1), IIII for instrument (HawkEye), YYYYMMDDTHHMMSS for date-time in year-month-day-T-hour-minute-second format, LLLL for level, SSSS for suite identifier ("oc" for ocean color), and VVVVVV for processing version ("V2022_0"): for example, "SEAHAWK1_HAWKEYE.20220903T183420.L2.OC.V2022_0.nc" (Fig. 3). Further details regarding the implementation of the NetCDF4 specification for NASA ocean color data are available at https://oceancolor.gsfc.nasa.gov/resources/docs/format/ (accessed 2-Jul-2024).
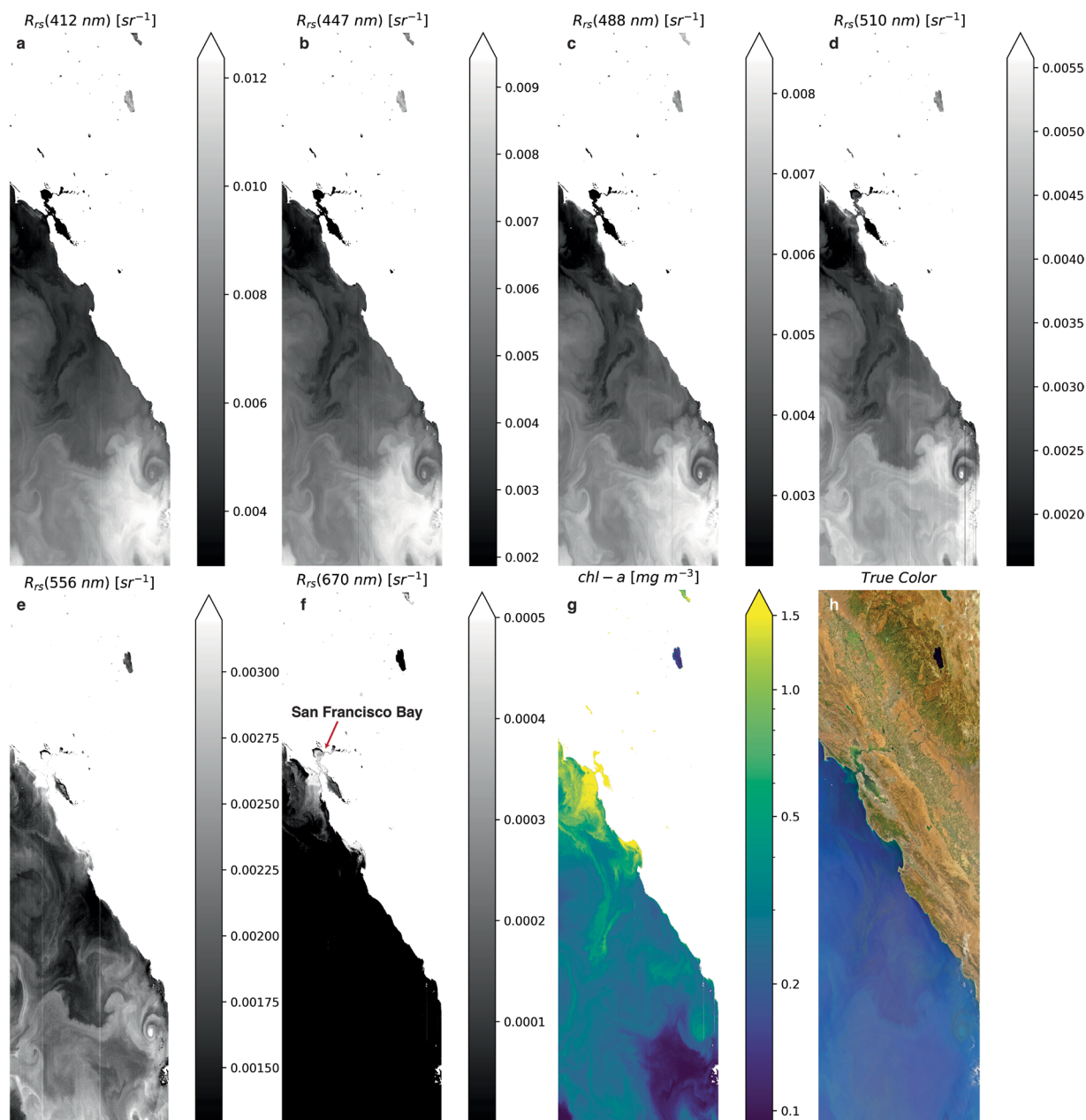
Fig. 3 (**a–f**) Level-2 remote sensing reflectance values (sr⁻¹) for the six bands in the visible part of the spectrum, as labeled, (**g**) chlorophyll-a (μg/L), and (**h**) true color image from file SEAHAWK1_HAWKEYE.20220903T183420.L2.OC.V2022_0.nc. Data from a HawkEye scene collected over primarily California, USA, and the California Current on 3-Sep-2022. San Francisco Bay, USA, is highlighted in F for reference.

Technical Validation

7,471 open-access research-grade images were collected during the mission. Images include raw radiance counts (i.e., in engineering units) as well as calibrated and geolocated at-aperture radiances (Level-1 or L1 data) at each band. Level-2 or L2 data comprise NASA's ocean color standard products or geophysical data (e.g., chlorophyll-a concentration, diffuse attenuation coefficient, remote sensing reflectances; see full list in Data Records).

Figure 3 depicts representative HawkEye data over the US West Coast and nearby waters on 3-Sep-2022. Shown here are L2 remote sensing reflectances from the visible portion of the spectrum, the chlorophyll-a product, and a true color image (i.e., using HawkEye's red, green, and blue bands after atmospheric correction). Spatially and spectrally variable aquatic signals are evident in the various bands, most clearly differing in the red (R_{rs}(670 nm)) where the CZCS atmospheric correction approach expects the ocean to be especially dark. However, it is worth noting that R_{rs}(670 nm) values climb to small but nonzero quantities in and just outside of San Francisco Bay, USA, where especially high suspended sediment concentrations result in higher reflectance values.
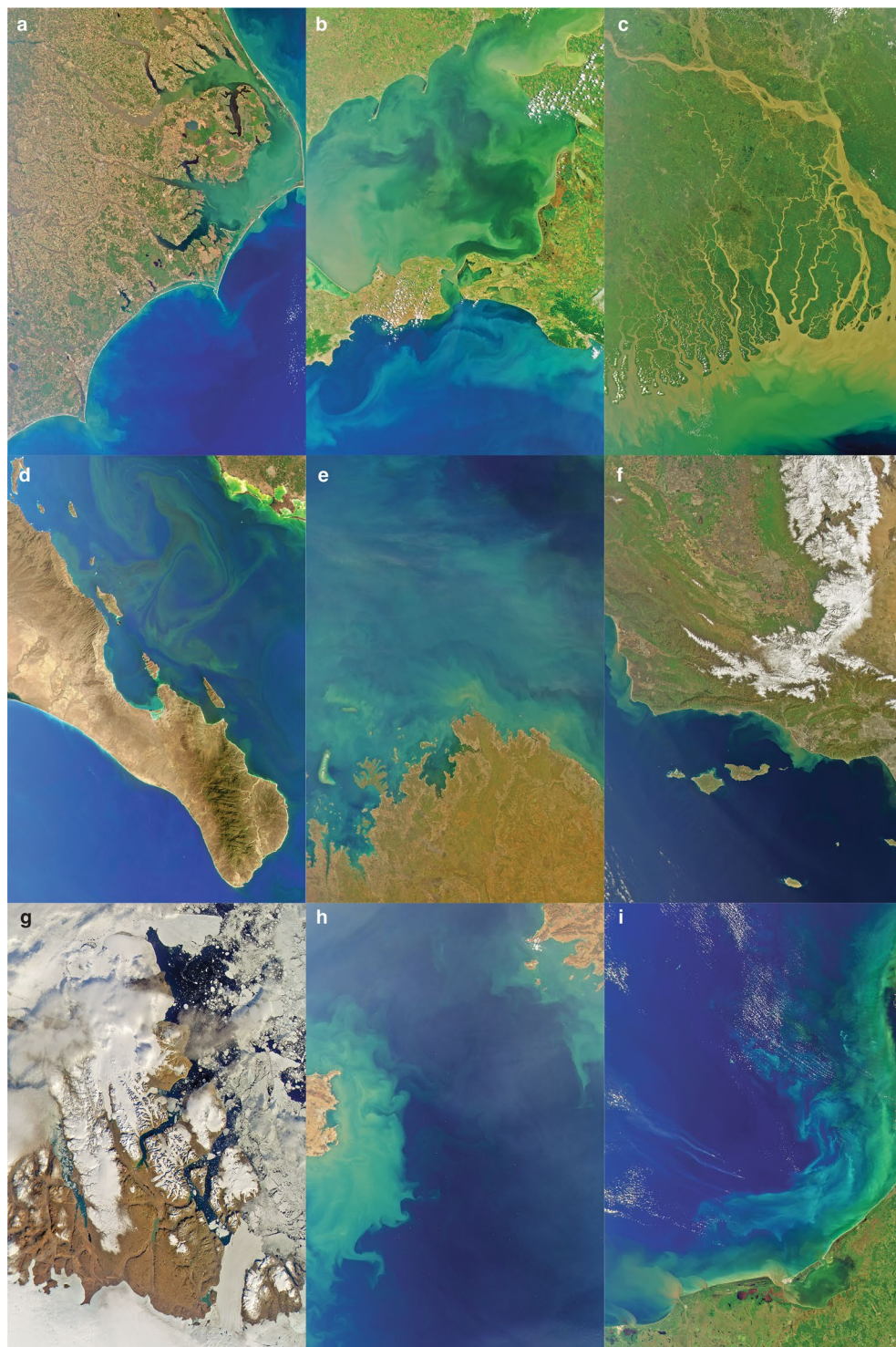
Fig. 4 Representative scenes from HawkEye, processed to "true color." (**a**), 28-Dec-2022; (**b**) Sea of Azov, 6-Jun-2023; (**c**) Bangladesh, 26-Oct-2022; (**d**) Baja California, 6-Jan-2023; (**e**) Northern Australia, 14-May-2023; (**f**) Santa Barbara, 2-Mar-2023; (**g**) Northeast Greenland, 26-Aug-2022; (**h**) Yellow Sea, 17-Nov-2022; (**i**) Western Yucatan, 11-Dec-2022.

The SeaHawk-HawkEye mission was intended as a proof-of-concept to demonstrate the possibility of integrating a comparatively low-cost ocean color imager of SeaWiFS quality using commercial off-the-shelf parts on a CubeSat. In achieving this goal, it also illustrates the potential scientific gains from a constellation of resolution ~100 m ocean color sensors, analogous to the Planet Labs approach for Earth imaging. Ocean color remote sensing at <1,000 m resolution is critical given the growing recognition of the importance of submesoscale processes (e.g., internal waves, Langmuir circulation, coastal upwelling, and eddies) on biophysical interactions, such as
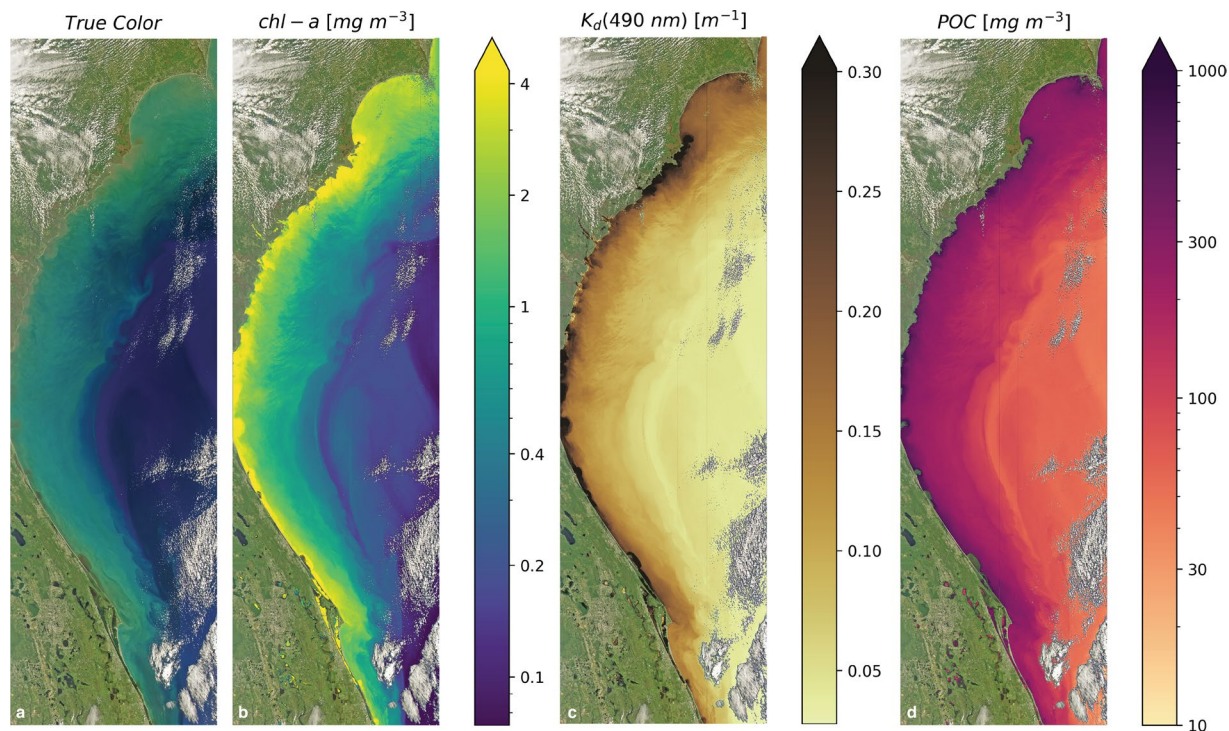
Fig. 5 (**a**) True color, (**b**) aquatic chlorophyll-a concentration, (**c**) diffuse attenuation coefficient at 490 nm, and (**d**) particulate organic carbon concentration in the South Atlantic Bight (Florida to North Carolina, USA) on 1-Oct-2022. (**b–d**) L2 aquatic data products overlaid on true color terrestrial imagery from HawkEye. Data from SEAHAWK1_HAWKEYE.20221001T152646.L2.OC.V2022_0.nc.
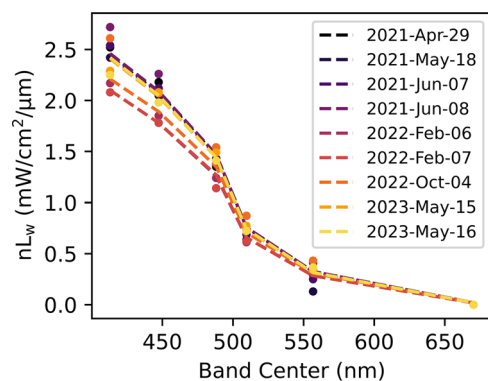

Fig. 6 Normalized water-leaving radiance (nL$_w$) vs. band center wavelength for nine HawkEye images of MOBY's location. HawkEye data are depicted as dots and MOBY climatological data are depicted as dashed lines; color represents date of imaging/*in-situ* climatology as shown in legend.

primary productivity[36] and thermal stress on sensitive ecosystems[37]. Furthermore, given recent improvements in harmonizing[38] and spatiotemporally fusing[39–42] remotely sensed imagery across varying spatial, temporal, and spectral scales, and the tradeoffs inherent to different approaches to satellite remote sensing, an optimal aquatic monitoring program would likely contain a mix of different satellite/sensor combinations, including the successors to SeaHawk-HawkEye. Figure 4 illustrates nine cropped scenes (full width of 1,800 pixels; cropped to 2,700 pixels in along-track dimension for ease of viewing) across the globe, demonstrating qualitatively HawkEye's powerful imagining capabilities.

As a representative example of processed HawkEye data products, Fig. 5 illustrates L2 chlorophyll-a, diffuse attenuation of light at 490 nm (a proxy for turbidity[14]), and particulate organic carbon in the waters off the US Southeast coast on 1-Oct-2022, one day after Hurricane Ian's departure from that region. Hurricane Ian was a catastrophic storm that made landfall in Cuba, southwest Florida, and South Carolina from 27–30 September 2022. In addition to the devastating loss of life and property, the impacts on water quality and carbon/nutrient cycling following severe storms due to increased terrestrial runoff and vertical mixing of the water column are
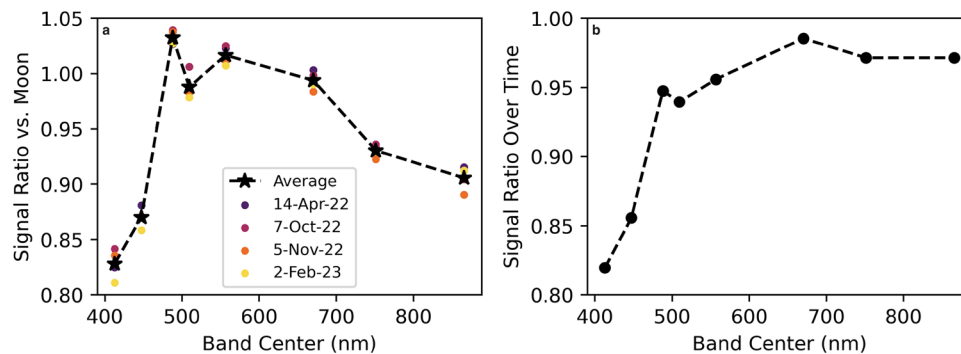
Fig. 7 (**a**) Signal response as a ratio of HawkEye signal divided by spectral radiance model's expected value vs. bands' center wavelengths. Signal ratio shown at four dates during which Moon imagery was collected and average value for each band. (**b**) Signal response as a ratio of HawkEye values for same bright location imaged two years apart vs. wavelengths.

substantial (e.g., Mallin, *et al.*[43], Paerl, *et al.*[44], and references therein). Figure 5 depicts clear and large gradients in each parameter in a cross-shore direction and turbidity (as indicated by $K_d(490\,nm)$) is especially elevated. Given the large spatial impact of such events, coupled with the need for high spatial resolution imagery in optically complex coastal waters, there is a need for data from HawkEye-like remote sensors.

Technical validation of the HawkEye dataset followed several ground and vicarious (in-space) procedures. The HawkEye sensor was designed and characterized prior to launch as described in the Methods and by Holmes, *et al.*[26]. Additionally, the measurement and application of a flat field correction using a calibration sphere from NASA (Labsphere 12" diameter, 4" diameter aperture, Spectralon interior, 4–35 W lamps operated at 3.07 A) mitigates pixel-to-pixel variability such that a uniform input would yield a uniform output. Without this flat field correction, minor differences between CCD pixels as well as dust streaks would result in artificial pixel-by-pixel offsets in the final calibrated signal, which could show up as visible streaks.

During the active mission, two key approaches were used for calibration/validation. First, the ocean color community standard vicarious calibration/validation approach for data collected at the Marine Optical BuoY (MOBY; 20°49.0'N, 157°11.5'W) was examined[45,46] (Fig. 6). As MOBY observations were not always available during HawkEye imaging at that location, a climatological time-series at the MOBY location was used to fill gaps. The climatology was calculated as described in Werdell, *et al.*[47]. Figure 6 illustrates strong correspondence of normalized water-leaving radiance for HawkEye data and MOBY *in-situ* climatological data over a two-year period aligning closely with the mission's operational window as described in Methods (21-Jun-2021–27-Oct-2023).

Second, SeaHawk was occasionally rotated to capture Moon imagery and a spectral radiance model of the Moon[48] was used to characterize HawkEye. Signal responses for each wavelength are shown as a ratio of spectral radiance model–calculated values for multiple lunar measurements in Fig. 7a. Bandwise correction factors are then calculated as the inverse of these ratios. There is a slight decrease in response over time, especially in the shorter (bluer) wavelengths, as confirmed also in Fig. 7b.

Several additional diagnostics were employed to determine the instrument's stability over time and signal quality. An analysis of dark frame data from the instrument, captured with the shutter closed, elucidated no changes in CCD dark currents or offsets, nor any accumulation of "dead" pixels. The most obvious change with the CCDs is the accumulation of a few dust particles over time. Since the CCD is windowless, a speck of dust landing on a 10 micron pixel can cause a large shift in sensitivity, and appears as a thin vertical dark line in the final image (see, especially, Figs. 3, 5). The impact of these particles on the data was mitigated by periodic updates to the flat field calibration tables.

Two images of the same ground location two years apart were collected, starting only two months after solar exposure began. In order to quantify change in signal quality, sensor response over a dry riverbed in Baja California was examined over two years (24-May-2019 to 23-May-2021; Fig. 7b). No real change in optical characteristics of this feature should have occurred, so any change in the received signal (after atmospheric and sun angle corrections) indicates sensor change. It is apparent that some loss of sensitivity has occurred in the blue portion of the spectrum, suspected to be the result of outgassing from either the Z306 black paint or the 2216 epoxy used in the manufacturing of the instrument and condensing on the optics. Direct solar ultraviolet illumination likely blackened the condensate, resulting in this blockage of $\approx 15\%$ of the signal.

As described in Methods, the instrument was designed to sum 3 channels of data to improve the SNR. However, the spacecraft's relative instability during operations resulted in these three samples appearing nine pixels apart which would have resulted in blurred imagery if combined as intended. Therefore, images only use one of the three channels, with a final SNR 60% of the design goal. However, the small 130 m pixels allow summing of nearby pixels to produce an image with resolution and SNR comparable to much larger ocean color instruments in areas of open ocean.

Additional details describing lessons learned in the development and use of the HawkEye imager can be found in Holmes, *et al.*[49].

Usage Notes

The SeaHawk-HawkEye mission demonstrated the ability to collect research-grade ocean color data from a CubeSat at a relatively low price and illuminates the potential scientific gains from a constellation of similar satellites. HawkEye collected imagery at higher spatial resolution than any other dedicated ocean color mission. All data are archived with NASA's OB.DAAC and remain freely available. Furthermore, NASA's Ocean Biology Processing Group maintains a log of reprocessing history at https://oceancolor.gsfc.nasa.gov/data/reprocessing/ (accessed 23-Jul-2024); any future releases of HawkEye data will be available and described there.

Code availability

NASA's freely available and widely used SeaDAS software and ocean color science software (ocssw) are used to process HawkEye data, the results of which comprise the majority of the analysis presented here. L1 processing utilizes v0.1.1, and L2 processing follows version 2022.0, as described in the NetCDF metadata for each file analyzed. Custom code for all remaining analysis is available at https://github.com/SUPScientist/SeaHawk-HawkEye_Analyses.

References

1. Yang, J. *et al.* The role of satellite remote sensing in climate change studies. *Nature Climate Change* **3**, 875–883, https://doi.org/10.1038/nclimate1908 (2013).
2. National Research Council. Assessing the Requirements for Sustained Ocean Color Research and Operations. https://doi.org/10.17226/13127 The National Academies Press, Washington, DC (2011).
3. IOCCG. *Why Ocean Colour? The Societal Benefits of Ocean-Colour Technology*. Reports of the International Ocean Colour Coordinating Group, Vol. 7 (Dartmouth, Canada, 2008).
4. United Nations. Resolution adopted by the General Assembly on 6 July 2017. 71/313. Work of the Statistical Commission pertaining to the 2030 Agenda for Sustainable Development (2017).
5. Gray, P. C. *et al.* Robust ocean color from drones: Viewing geometry, sky reflection removal, uncertainty analysis, and a survey of the Gulf Stream front. *Limnology and Oceanography: Methods* **20**, 656–673, https://doi.org/10.1002/lom3.10511 (2022).
6. Windle, A. E. & Silsbe, G. M. Evaluation of Unoccupied Aircraft System (UAS) Remote Sensing Reflectance Retrievals for Water Quality Monitoring in Coastal Waters. *Frontiers in Environmental Science* **9**, https://doi.org/10.3389/fenvs.2021.674247 (2021).
7. Román, A., Heredia, S., Windle, A. E. & Tovar-Sánchez, A. & Navarro, G. Enhancing Georeferencing and Mosaicking Techniques over Water Surfaces with High-Resolution Unmanned Aerial Vehicle (UAV) Imagery. *Remote Sensing* **16**, 290 (2024).
8. McClain, C. R., Franz, B. A. & Werdell, P. J. Genesis and Evolution of NASA's Satellite Ocean Color Program. *Frontiers in Remote Sensing* **3**, https://doi.org/10.3389/frsen.2022.938006 (2022).
9. Behrenfeld, M. J. & Falkowski, P. G. Photosynthetic rates derived from satellite-based chlorophyll concentration. *Limnology and Oceanography* **42**, 1–20, https://doi.org/10.4319/lo.1997.42.1.0001 (1997).
10. Behrenfeld, M. J. *et al.* Climate-driven trends in contemporary ocean productivity. *Nature* **444**, 752–755, https://doi.org/10.1038/nature05317 (2006).
11. Kulk, G. *et al.* Primary Production, an Index of Climate Change in the Ocean: Satellite-Based Estimates over Two Decades. *Remote Sensing* **12**, 826 (2020).
12. Brewin, R. J. W. *et al.* Sensing the ocean biological carbon pump from space: A review of capabilities, concepts, research gaps and future developments. *Earth-Science Reviews* **217**, 103604, https://doi.org/10.1016/j.earscirev.2021.103604 (2021).
13. Jönsson, B. F., Kulk, G. & Sathyendranath, S. Review of algorithms estimating export production from satellite derived properties. *Frontiers in Marine Science* **10**, https://doi.org/10.3389/fmars.2023.1149938 (2023).
14. Shi, W. & Wang, M. Characterization of global ocean turbidity from Moderate Resolution Imaging Spectroradiometer ocean color observations. *Journal of Geophysical Research: Oceans* **115**, https://doi.org/10.1029/2010JC006160 (2010).
15. Morel, A. & Bélanger, S. Improved detection of turbid waters from ocean color sensors information. *Remote Sensing of Environment* **102**, 237–249, https://doi.org/10.1016/j.rse.2006.01.022 (2006).
16. Wei, J. *et al.* Global Estimation of Suspended Particulate Matter From Satellite Ocean Color Imagery. *Journal of Geophysical Research: Oceans* **126**, e2021JC017303, https://doi.org/10.1029/2021JC017303 (2021).
17. Pahlevan, N. *et al.* Seamless retrievals of chlorophyll-a from Sentinel-2 (MSI) and Sentinel-3 (OLCI) in inland and coastal waters: A machine-learning approach. *Remote Sensing of Environment* **240**, 111604, https://doi.org/10.1016/j.rse.2019.111604 (2020).
18. Kuhn, C. *et al.* Performance of Landsat-8 and Sentinel-2 surface reflectance products for river remote sensing retrievals of chlorophyll-a and turbidity. *Remote Sensing of Environment* **224**, 104–118, https://doi.org/10.1016/j.rse.2019.01.023 (2019).
19. Pahlevan, N., Chittimalli, S. K., Balasubramanian, S. V. & Vellucci, V. Sentinel-2/Landsat-8 product consistency and implications for monitoring aquatic systems. *Remote Sensing of Environment* **220**, 19–29, https://doi.org/10.1016/j.rse.2018.10.027 (2019).
20. Pahlevan, N. *et al.* Landsat 8 remote sensing reflectance (Rrs) products: Evaluations, intercomparisons, and enhancements. *Remote Sensing of Environment* **190**, 289–301, https://doi.org/10.1016/j.rse.2016.12.030 (2017).
21. Pahlevan, N., Sarkar, S., Franz, B. A., Balasubramanian, S. V. & He, J. Sentinel-2 MultiSpectral Instrument (MSI) data processing for aquatic science applications: Demonstrations and validations. *Remote Sensing of Environment* **201**, 47–56, https://doi.org/10.1016/j.rse.2017.08.033 (2017).
22. Vanhellemont, Q. Daily metre-scale mapping of water turbidity using CubeSat imagery. *Opt. Express* **27**, A1372–A1399, https://doi.org/10.1364/OE.27.0A1372 (2019).
23. Vanhellemont, Q. Evaluation of eight band SuperDove imagery for aquatic applications. *Opt. Express* **31**, 13851–13874, https://doi.org/10.1364/OE.483418 (2023).
24. Manzo, C., Bresciani, M., Giardino, C., Braga, F. & Bassani, C. Sensitivity analysis of a bio-optical model for Italian lakes focused on Landsat-8, Sentinel-2 and Sentinel-3. *European Journal of Remote Sensing* **48**, 17–32, https://doi.org/10.5721/EuJRS20154802 (2015).
25. Planet Team. *Planet application program interface: In space for life on Earth*, https://api.planet.com/ (2017).
26. Holmes, A., Morrison, J., Feldman, G., Patt, F. & Lee, S. Hawkeye ocean color instrument: performance summary. *SPIE Optical Engineering + Applications Proceedings* **10769**, https://doi.org/10.1117/12.2320654 (2018).
27. Baith, K., Lindsay, R., Fu, G. & McClain, C. R. Data analysis system developed for ocean color satellite sensors. *Eos, Transactions American Geophysical Union* **82**, 202–202, https://doi.org/10.1029/01EO00109 (2001).
28. Gordon, H. R. & Wang, M. Retrieval of water-leaving radiance and aerosol optical thickness over the oceans with SeaWiFS: a preliminary algorithm. *Appl. Opt.* **33**, 443–452, https://doi.org/10.1364/AO.33.000443 (1994).
29. Gordon, H. R. Evolution of Ocean Color Atmospheric Correction: 1970–2005. *Remote Sensing* **13**, 5051, https://doi.org/10.3390/rs13245051 (2021).

30. Gregg, W. W. *et al.* NOAA-NASA Coastal Zone Color Scanner Reanalysis Effort. *Appl. Opt.* **41**, 1615–1628, https://doi.org/10.1364/AO.41.001615 (2002).

31. IOCCG. *Remote Sensing of Inherent Optical Properties: Fundamentals, Tests of Algorithms, and Applications.* Reports of the International Ocean Colour Coordinating Group, Vol. 5 (Dartmouth, Canada, 2006).

32. Werdell, P. J. *et al.* An overview of approaches and challenges for retrieving marine inherent optical properties from ocean color remote sensing. *Progress in Oceanography* **160**, 186–212, https://doi.org/10.1016/j.pocean.2018.01.001 (2018).

33. O'Reilly, J. E. & Werdell, P. J. Chlorophyll algorithms for ocean color sensors - OC4, OC5 & OC6. *Remote Sensing of Environment* **229**, 32–47, https://doi.org/10.1016/j.rse.2019.04.021 (2019).

34. NASA Goddard Space Flight Center, Ocean Ecology Laboratory, Ocean Biology Processing Group. HawkEye-SeaHawk L1 Data, Version 1. NASA OB.DAAC, Greenbelt, MD, USA. https://doi.org/10.5067/SEAHAWK-1/HawkEye/L1A/DATA/1. Accessed on 26-Jun-2024.

35. NASA Goddard Space Flight Center, Ocean Ecology Laboratory, Ocean Biology Processing Group. HawkEye-SeaHawk L2 Data, Version 2022.0. NASA OB.DAAC, Greenbelt, MD, USA. https://doi.org/10.5067/SEAHAWK-1/HawkEye/L2/OC/2022.0. Accessed on 26-Jun-2024.

36. Mahadevan, A. The Impact of Submesoscale Physics on Primary Productivity of Plankton. *Annual review of marine science* **8**, 161–184, https://doi.org/10.1146/annurev-marine-010814-015912 (2016).

37. McWhorter, J. K. *et al.* Mesoscale Eddies Influence Coral Reef Environments in the Northwest Gulf of Mexico. *Journal of Geophysical Research: Oceans* **129**, e2023JC020821, https://doi.org/10.1029/2023JC020821 (2024).

38. Claverie, M. *et al.* The Harmonized Landsat and Sentinel-2 surface reflectance data set. *Remote Sensing of Environment* **219**, 145–161, https://doi.org/10.1016/j.rse.2018.09.002 (2018).

39. Song, H., Liu, Q., Wang, G., Hang, R. & Huang, B. Spatiotemporal Satellite Image Fusion Using Deep Convolutional Neural Networks. *IEEE Journal of Selected Topics in Applied Earth Observations and Remote Sensing* **11**, 821–829, https://doi.org/10.1109/JSTARS.2018.2797894 (2018).

40. Li, J. *et al.* Deep learning in multimodal remote sensing data fusion: A comprehensive review. *International Journal of Applied Earth Observation and Geoinformation* **112**, 102926, https://doi.org/10.1016/j.jag.2022.102926 (2022).

41. Wang, Q. & Atkinson, P. M. Spatio-temporal fusion for daily Sentinel-2 images. *Remote Sensing of Environment* **204**, 31–42, https://doi.org/10.1016/j.rse.2017.10.046 (2018).

42. Xiao, J. *et al.* A review of remote sensing image spatiotemporal fusion: Challenges, applications and recent trends. *Remote Sensing Applications: Society and Environment* **32**, 101005, https://doi.org/10.1016/j.rsase.2023.101005 (2023).

43. Mallin, M. A. *et al.* Hurricane effects on water quality and benthos in the Cape Fear watershed: natural and anthropogenic impacts. *Ecological Applications* **9**, 350–362, https://doi.org/10.1890/1051-0761(1999)009[0350:HEOWQA]2.0.CO;2 (1999).

44. Paerl, H. W. *et al.* Recent increase in catastrophic tropical cyclone flooding in coastal North Carolina, USA: Long-term observations suggest a regime shift. *Scientific reports* **9**, 10620, https://doi.org/10.1038/s41598-019-46928-9 (2019).

45. Clark, D. K. *et al.* Validation of atmospheric correction over the oceans. *Journal of Geophysical Research: Atmospheres* **102**, 17209–17217, https://doi.org/10.1029/96JD03345 (1997).

46. Bailey, S. W., Hooker, S. B., Antoine, D., Franz, B. A. & Werdell, P. J. Sources and assumptions for the vicarious calibration of ocean color satellite observations. *Appl. Opt.* **47**, 2035–2045, https://doi.org/10.1364/AO.47.002035 (2008).

47. Werdell, P. J., Bailey, S. W., Franz, B. A., Morel, A. & McClain, C. R. On-orbit vicarious calibration of ocean color sensors using an ocean surface reflectance model. *Appl. Opt.* **46**, 5649–5666, https://doi.org/10.1364/AO.46.005649 (2007).

48. Kieffer, H. H. & Stone, T. C. The Spectral Irradiance of the Moon. *The Astronomical Journal* **129**, 2887, https://doi.org/10.1086/430185 (2005).

49. Holmes, A. *et al.* Lessons Learned from the HawkEye-SeaHawk Mission. *Zenodo* https://doi.org/10.5281/zenodo.12797354 (2024).

Acknowledgements

Author contributions

All authors contributed extensively to the work presented in this paper. P.J.B. analyzed data, wrote the manuscript, and directs the current phase of the project. S.R.C. analyzed data and is co-PI of the current phase of the project. J.M. supervised the prior phase of the project which resulted in design, fabrication, launch, and operationalization of the mission. G.F. directed the team at NASA that enabled the mission's success. A.H. directed the team at Cloudland Instruments that built and characterized the HawkEye imager and resulting data. S.B., A.S., L.H., F.P., N.K. and C.R. led spacecraft analysis, image acquisition, and image data calibration, processing, and archiving. C.C., J.C., B.L., H.G., A.B. and R.G. led spacecraft design and fabrication and flight operations.

Competing interests

The authors declare no competing interests.

Additional information

Correspondence and requests for materials should be addressed to P.J.B.

Reprints and permissions information is available at www.nature.com/reprints.

Publisher's note Springer Nature remains neutral with regard to jurisdictional claims in published maps and institutional affiliations.